Applied Catalysis B: Environmental 100 (2010) 84–90

Contents lists available at ScienceDirect

Applied Catalysis B: Environmental

journal homepage: www.elsevier.com/locate/apcatb

Enhanced visible light photocatalytic activity of N-doped TiO_2 in relation to single-electron-trapped oxygen vacancy and doped-nitrogen

Yan Wang[a,b], Caixia Feng[a,c], Min Zhang[a], Jianjun Yang[a,*], Zhijun Zhang[a]

[a] Key Laboratory for Special Functional Materials, Henan University, Kaifeng 475004, China
[b] Functional Material Research Center, Kaifeng University, Kaifeng 475004, China
[c] Institute of Environmental and Analytical Sciences, College of Chemistry and Chemical Engineering, Henan University, Kaifeng 475004, China

ARTICLE INFO

Article history:
Received 17 June 2010
Received in revised form 6 July 2010
Accepted 13 July 2010
Available online 21 July 2010

Keywords:
N-doped TiO_2
Catalyst
Visible light photocatalytic activity
Single-electron-trapped oxygen vacancy

ABSTRACT

Although numerous papers are available about the origin of visible light photocatalytic activity of N-doped TiO_2, it still remains conflicting how nitrogen-doping affects the visible light photocatalytic activity of TiO_2. Thus N-doped TiO_2 was prepared by heat treatment of commercial P25-TiO_2 in flowing NH_3, aiming at revealing the origin of visible light sensitization of N-doped TiO_2. The resulting N-doped TiO_2 was characterized by means of electron spin resonance (ESR), X-ray photoelectron spectroscopy (XPS), diffusion reflectance spectrometry (DRS), and X-ray diffraction (XRD). Results indicate that N-doped TiO_2 shows triplet *g* value ESR signals ($g = 1.987$, 2.004 and 2.024), which is attributed to single-electron-trapped oxygen vacancy (denoted as SETOV) in a certain chemical environment. Its visible light photocatalytic activity is proportional to the intensity of the triplet *g* value signals, which implies that the visible light photocatalytic activity of N-doped TiO_2 is closely correlated to the formation of SETOV during heat treatment in flowing NH_3. Besides, N-doped TiO_2 catalyst calcinated at 600 °C possesses the highest photocatalytic activity, but that calcinated at 700 °C has drastically decreased photocatalytic activity and shows no XPS signal of nitrogen. Moreover, N-doped TiO_2 shows visible light absorption in a wavelength range of 400–520 nm, which is attributed to the formation of SETOV and phase transformation from anatase to rutile. It is suggested that the visible light photocatalytic activity of N-doped TiO_2 is co-determined by the formation of SETOV in TiO_2 matrix and existence of doped-N on the surface. In other words, in the absence of either SETOV in TiO_2 matrix or doped-nitrogen on the surface, N-doped TiO_2 will not show visible light photocatalytic activity; and the higher the SETOV concentration is, the better the visible light photocatalytic activity will be.

1. Introduction

There have been numerous reports on the photoabsorption and photocatalytic properties of N-doped TiO_2 in visible light region. In 1986, Sato reported for the first time that N-doped TiO_2 obtained by annealing $Ti(OH)_4$ mixed with NH_4Cl or NH_4OH showed visible light photocatalytic activity [1]. He ascribed the visible light sensitization to NO_x impurities in the TiO_2 lattice. Asahi and coworkers, based on theoretical analysis, attributed the visible light photocatalytic activity of N-doped TiO_2 to the formation of Ti–N bond, as evidenced by XPS spectrum of N 1*s* at 396 eV [2]. Irie and coworkers systematically studied the relationship between the amount of doped-nitrogen and photocatalytic activity of N-doped TiO_2 for photooxidation of 2-propanol under visible light and ultraviolet irradiation [3]. They also suggested that the N 1*s* chemical state at 396 eV of N-doped TiO_2 is due to visible light response. In 2003, Ihara and coworkers obtained N-doped TiO_2 with visible light activity by hydrolyzing $Ti(SO_4)_2$ in aqueous ammonia and follow-up calcinating at 400 °C in air; and they suggested that oxygen-deficiency is essentially indispensable for visible light sensitization of N-doped TiO_2, while doped-N with a low content functions to retard the reoxidation of oxygen-deficient TiO_2 [4]. Since then, various methods have been established for nitrogen-doping of TiO_2; and sol–gel method [4–8], treatment of TiO_2 (particles or nanotube) by gases under high temperature [3,9–14], and ion implantation of TiO_2 [15–17] are the three kinds of most representative ones.

At the same time, some researchers have investigated the chemical state of doped-nitrogen by means of ESR [18–20]. For example, Giamello and coworkers reported a novel N-doped TiO_2 containing two different types of paramagnetic species, i.e., neutral NO radical and NO_2^{2-} radical ion; and they attributed the visible light activity of N-doped TiO_2 to the two types of nitrogen-containing species [18]. Gole and coworkers obtained titania-based oxynitride structures at room temperature *via* direct nitridation of porous

* Corresponding author. Tel.: +86 378 3881358; fax: +86 378 3881358.
E-mail address: yangjianjun@henu.edu.cn (J. Yang).

0926-3373/$ – see front matter © 2010 Elsevier B.V. All rights reserved.
doi:10.1016/j.apcatb.2010.07.015

TiO_2 nanocolloids in the presence of alkyl ammonium compounds and found that the products showed electron spin resonance, with increased intensity after nitridation, at $g = 2.0035$ [19]. They attributed the resonance to an oxygen hole center created near the surface of the nanocolloid, and ascribed the visible light sensitization of N-doped TiO_2 to the oxygen hole center. Giamello and coworkers, based on ESR and DRS analyses as well as theoretical approach, suggested that the triplet ESR signal of N-doped TiO_2 was assigned to $N^{\bullet}$ center (single nitrogen atom center in bulk TiO_2) as the origin of photoactivity [20]. Unfortunately, the source of the photoactivity of N-doped TiO_2 in visible light region is still an open subject of controversy. Briefly, three mechanisms have been proposed to account for visible light activity of N-doped TiO_2. Asahi et al. proposed that N atom was doped into substitutional sites of TiO_2 resulting in visible light response [2]. Ihara et al. suggested that oxygen vacancies benefit to visible light photo-response are introduced in TiO_2 during preparation of samples and doped-nitrogen acts as a blocker for reoxidation of oxygen vacancies [4]. Prokes et al., Livraghi et al., and Nakamura et al. separately proposed that the visible light response of N-doped TiO_2 arises from electronic transitions from localized states to conduction band [19–22]. Generally speaking, it has been widely accepted that nitrogen-doping leads to narrowing of TiO_2 band gap *via* mixing N 2*p* orbital and O 2*p* orbital and hence visible light photocatalytic activity [2,20–22]. However, Serpone et al. proposed that the visible light photocatalytic activity of N-doped TiO_2 was originated from color centers (F-centers) [23–25]. Recently, Jin et al. prepared N-doped TiO_2 with high visible light photocatalytic activity by treating nanotube titanic acid in flowing NH_3 and they believed that $Ti–V_o^{\bullet}–NO$ was the active center [10–12,26].

In the present work, N-doped TiO_2 were prepared by annealing commercial P25-TiO_2 in NH_3 flow at different temperatures. The products were characterized by means of ESR, XPS, DRS and XRD. The photocatalytic activity of P25-TiO_2 and N-doped samples for photooxidation of propylene under visible light irradiation ($\lambda \geq 420$ nm) was measured. In connection with ESR and XPS results, we suppose that the visible light activity of N-doped TiO_2 is co-determined by the formation of SETOV and the existence of doped-N on the surface; and the higher the SETOV concentration is the better the visible light photocatalytic activity will be.

2. Experimental

2.1. Preparation of samples

N-doped TiO_2 (anatase/rutile) was prepared by thermal-treatment of commercial P25-TiO_2 in NH_3 flow (99.9%) at 400–700 °C for 4 h, which was carried out in a tubular furnace (the resulting samples are denoted as N-P25(400–700) for convenience). Typically, about 1.0 g of P25-TiO_2 was homogeneously placed in a ceramic container and heated in tubular furnace. Prior to calcinations, NH_3 flow was inlet for 30 min to remove air in the furnace. After being annealed at 400–700 °C for 4 h and cooled naturally to room temperature, N-doped TiO_2 samples were obtained.

2.2. Characterizations

Diffusion reflectance spectra (DRS) were obtained on a Shimadzu U-3010 spectrometer, using $BaSO_4$ as a reference. X-ray diffraction (XRD) patterns were measured on an X'Pert Philips diffractometer (Cu Kα radiation; 2θ range 10–90°, step size 0.02°, accelerating voltage 40 kV, applied current 40 mA). Electron spin resonance (ESR) spectra were obtained on a Brüker ESP 300E apparatus (operated in X band: ca. 9.80 kHz) at a field modulation of 100 kHz, an amplitude modulation of 0.2 mT and a microwave power of 10 mW (the measurement was performed at room temperature and in ambient air, without vacuum-pumping). The *g*-tensors of the ESR signals were obtained by setting *g* of diphenyl picryl hydrazyl (DPPH), 2.0036, as reference. X-ray photoelectron spectra (XPS) were recorded with a Kratos AXIS Ultra spectrometer using monochromatized Al Kα ($h\nu = 1486.6$ eV) radiation as the excitation source (power 150 W: 15 kV and 10 mA). The C 1*s* of hydrocarbon at 284.8 eV was used as an internal standard for the correction of charging shift. The pressure of sample analysis chamber (SAC) during data acquisition was kept below 10^{-8}–10^{-9} torr. The survey spectra and core level spectra were collected at pass energy of 80 eV and 40 eV, respectively.

2.3. Evaluation of visible light photocatalytic activity

The photocatalytic activity of P25-TiO_2 and N-P25(400–700) was evaluated by monitoring oxidation of propylene under visible light irradiation. About 30 mg of each sample was spread on one side of a roughened glass plate (ca. 10 cm^2) located in a flat quartz tube reactor. A 500 W xenon lamp was used as the visible light source. Between the xenon lamp and reactor were inserted a cut filter ($\lambda \geq 420$ nm) and a water cell to eliminate ultraviolet and infrared light; and the intensity of the light with $\lambda \geq 420$ nm irradiated on to-be-tested samples was ca. 0.4 mW/cm^2. Pure C_3H_6 (99.99%) stored in a high-pressure cylinder and air was used as the feed gas (flow rate 100 mL h^{-1}). The concentration of C_3H_6, *C*, was determined at a sensitivity of 1 ppm V using a chromatograph (Shimadzu GC-9A) equipped with a flame ionization detector (FID), a GDX-502 column, and a reactor loaded with Ni catalyst for the methanization of CO_2. The removal rate of C_3H_6 was calculated as $(C_0 - C)/C_0 \times 100\%$; where C_0 refers to the concentration of feed gas C_3H_6 and is equal to 600 ppm V.

3. Results and discussion

The visible light photocatalytic activity of P25-TiO_2 and N-P25(400–700) samples evaluated by measuring the percentage removal of propylene in association with the conversion rate of CO_2 is shown in Fig. 1. It can be seen that P25-TiO_2 and N-P25(400) have no visible light photocatalytic activity, and naturally their CO_2 conversion rate is 0%. Sample N-P25(500) calcinated at 500 °C has a removal rate of 3.1 for propylene; and sample N-P25(600) calcinated at 600 °C has the maximum removal rate of 7.3 for propylene.

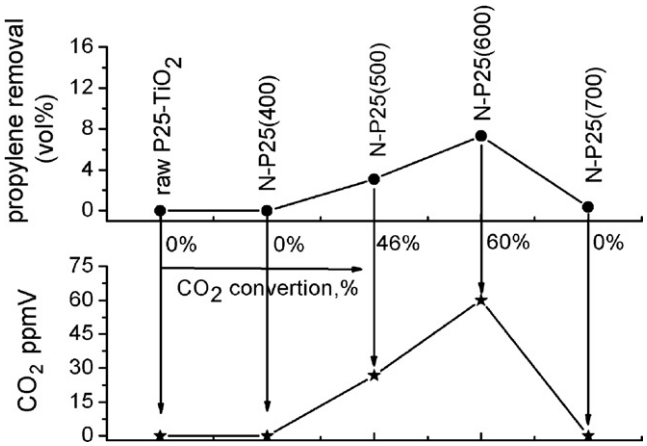

Fig. 1. Visible light photocatalytic activity of P25 and N-P25(400–700) in association with conversion rate of CO_2. Visible light source: 500 W Xenon lamp, between the Xenon lamp and the reactor were inserted a cut filter with $\lambda \geq 420$ nm and a water cell to eliminate UV and infrared light. The light intensity of $\lambda \geq 420$ nm irradiated on sample is ca. 0.4 mW/cm^2.

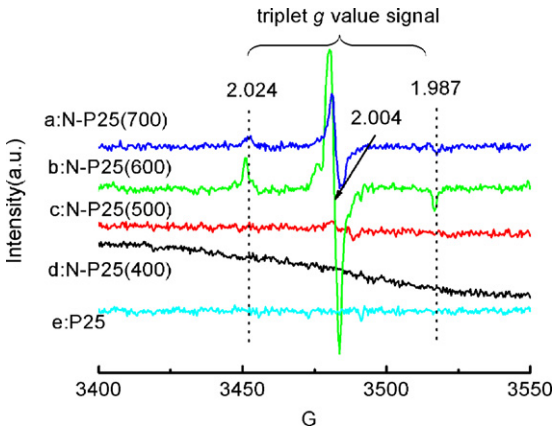

Fig. 2. ESR spectra of P25 and N-P25(400–700) measured at room temperature in atmosphere.

However, sample N-P25(700) calcinated at 700 °C has almost no visible light photocatalytic activity (nearly zero), and its CO_2 conversion rate is 0% (undetectable by gas chromatograph). Noticing that 1 mol C_3H_6 should produce 3 mol CO_2 under condition of complete oxidation but the selectivity of CO_2 formation calculated for N-P25(500) and N-P25(600) is about 46% and 60%, respectively, we can infer that propylene is not completely converted into CO_2 *via* photocatalytic oxidation in the present system.

Fig. 2 displays the ESR spectra of P25-TiO_2 and N-P25(400–700). Samples P25-TiO_2 and N-P25(400) do not show any ESR signals, meaning that they are free of paramagnetic species. After being treated in flowing NH_3 at $T \geq 500$ °C, the resultant catalyst samples show triplet *g* value signals ($g = 1.987$, 2.004 and 2.024); but no Ti^{3+} ESR signal ($g = 1.96$) is detected, well conforming to Ti *2p* XPS spectra shown in Fig. 7. Early in 1968, Sancier and coworkers reported similar triplet *g* value signals of white anatase TiO_2 prepared by calcinations of ammonia solution-hydrolyzed product of $TiCl_4$ at 500 °C in oxygen stream [27]. They found that white anatase TiO_2 pretreated in vacuum under 500 °C turned into bluish gray and showed *g* value signals at $g = 2.002$ and 1.93 only at low temperature (e.g., −195 °C) and in vacuum condition, which were assigned to O^- and Ti^{3+} species, respectively. When the bluish gray TiO_2 sample was heated at 500 °C in oxygen, its color became pale yellow, while the *g* value signals at $g = 2.002$ and $g = 1.93$ disappeared in association with emerge of triplet *g* value signals at $g = 1.984$, 2.004, and 2.023, exactly the same as that shown in Fig. 2. Sancier and coworkers ascribed the triplet as a solid state defect but not identified the paramagnetic species. In 1971, Iyengar and coworkers re-studied the triplet *g* value signals of anatase TiO_2 and assigned them to paramagnetic nitrogen oxides (such as NO, NO_2, NO_2^-, NO_2^{2-}) [28,29]. Recently, similar triplet *g* value ESR signals of N-doped TiO_2 have been reported [18–20,30,31]. Domen and coworkers prepared visible light sensitized $La_{0.5}$–N–TiO_2 photocatalyst by making use of "polymerized complex" method and detected triplet *g* value signals under visible light irradiation in evacuation condition at 77 K [30]. They assigned the triplet to some paramagnetic nitrogen oxides and supposed that the visible light absorption and photocatalytic activity of $La_{0.5}$–N–TiO_2 photocatalyst was attributed to paramagnetic N species. In 2004, Giamello and coworkers prepared N-doped TiO_2 by thermal-treatment of the hydrolysis product of titanium (IV) isopropoxide with aqueous NH_4Cl at 770 K in air; they attributed the triplet *g* value signal to NO_2^{2-} radical anion which deeply interacts with the oxide and distributes more than half of its spin density in a *p* orbital of the nitrogen atom [18]. However, the possible assignment of the triplet *g* value signal to NO_2^{2-} radical ion was afterwards discarded by them, since this species was computed (with density function theory calculations) to be unstable in bulk TiO_2 [31]. In follow-up systematical investigation of N-doped TiO_2 (anatase) by means of ESR and DRS analyses as well as theoretical approach [20], they assigned the triplet *g* value signal to paramagnetic ($N_b^\bullet$) bulk centers (single atom nitrogen centers in bulk TiO_2) and proposed that the origin of visible light photoactivity of N-doped TiO_2 is attributed to $N_b^\bullet$ centers. In 2009, Giamello and coworkers reported the paramagnetic species in the bulk of N-doped rutile TiO_2 [32]. They ascribed the paramagnetic species to an interstitial N atom stick to a O^{2-} lattice ion but not a N substituting O^{2-} in the lattice. Previously we reported similar triplet signal of N-doped anatase TiO_2 prepared by heat-treatment of nanotube titanic acid in NH_3 flow and attributed the main peak in the triplet ($g = 2.004$) to single electron associated with oxygen vacancy (SETOV) [10–12,26]. The two weak satellite peaks ($g = 2.024$, 1.987) were assigned to the perturbation peaks of the triplet, and the triplet *g* value signal was identified as Ti–$V_o^\bullet$–NO leading to enhanced visible light photocatalytic activity. What should be emphasized is that doped-N has not been detected by XPS for sample N-P25(700) in the present research although it has triplet signal (see Fig. 6). This means that further investigation is imperative before assigning the triplet of the N-doped TiO_2 to Ti–$V_o^\bullet$–NO. It has been well known that oxygen vacancies of TiO_2 can be obtained by way of reduction with H_2 or heat-treatment in vacuum [33–40]. However, the resultant oxygen vacancies are unstable against reoxidation. Naccache and coworkers observed a symmetrical ESR signal with $g = 2.003$ on slightly reduced TiO_2 and attributed it to the localization of a conduction electron in the lattice [33,34]. Volodin and coworkers detected an ESR signal with $g = 2.004$ for reduced anatase and ascribed it to the surface defects [35,36]. A typical ESR spectrum of TiO_2 after reduction in vacuo, registered at 77K was given by Serwicka et al. [37,38]. A sharp signal with $g = 2.003$ was attributed to a bulk defect, probably an electron trapped on an oxygen vacancy, i.e., SETOV. Ihara prepared a visible light active TiO_2 photocatalyst by RF-plasma treatment and observed the symmetrical ESR signal at $g = 2.003$ in the RF-plasma-heat-treated TiO_2 [39,40]. They assigned it to electrons trapped at oxygen-defect site, also can be denoted as SETOV. Considering ammonia gas with weak alkalinity and liability to partly decompose into H_2 and N_2 above 480 °C, the NH_3-heat-treatment of P25-TiO_2 is hopefully to result in a slightly reduced N-doped TiO_2 whose triplet *g* value ESR signal are shown in Fig. 2. Combined with the above literature data, the triplet ESR signal should be identified as SETOV, while other two weak satellite peaks can be ascribed to the perturbation peaks of the triplet resulting from the strong interaction between SETOV.

Noticing that the intensity of ESR signal is directly proportional to the concentration of paramagnetic species, we can summarize the intensity of the triplet signal in relation to visible light photocatalytic activity (Fig. 1) as a function of heat-treatment temperature in flowing NH_3. As shown in Fig. 3, the intensity of the triplet signal varies in a wave-like manner with varying temperature: it initially increases from N-P25(400) to N-P25(600) and then it decreases from N-P25(600) to N-P25(700), corresponding to the variation of the concentration of SETOV in the same manner. Besides, the visible light photocatalytic activity is in line with the intensity of the triplet signal, i.e., the concentration of SETOV. This means that the visible light photocatalytic activity of N-doped TiO_2 is attributed to the formation of SETOV during heat-treatment in flowing NH_3. The absence of the ESR signals for samples P25-TiO_2 and N-P25(400) well corresponds to their lowered visible light photocatalytic activity, and the maximum concentration of SETOV for sample N-P25(600) is proportional to its best visible light photocatalytic activity. What should be pointed out is that the visible light photocatalytic activity of sample N-P25(700) suddenly decreases to almost 0, though it has a large number of SETOV. This implies that formation of high enough concentration of SETOV is not the

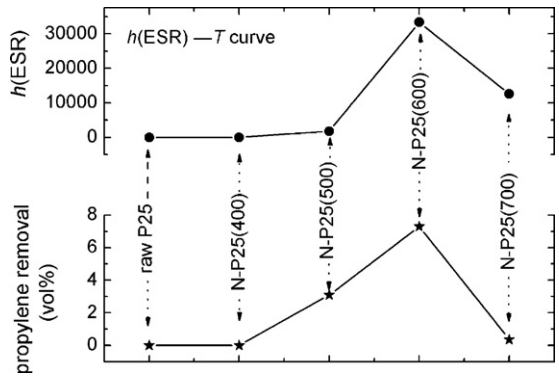

Fig. 3. Intensity of triplet *g* value signal in association with visible light photocatalytic activity of P25 and N-doped TiO_2 samples. *h*(ESR) refers to the signal intensity at *g* = 2.004.

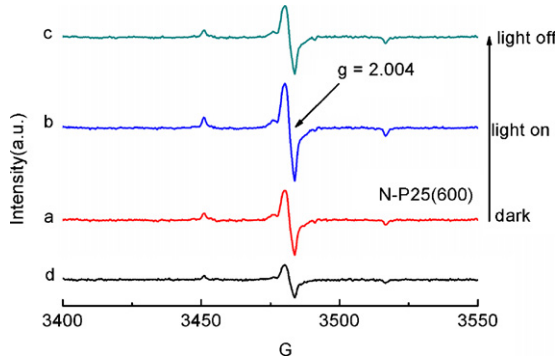

Fig. 4. ESR spectra of N-P25(600) obtained in the dark (a), under light irradiation (532 nm) for 9 min (b), after turning off light for 9 min (c), and after subtracting c from b (d).

sole factor determining the visible light photocatalytic activity of N-doped TiO_2 prepared via reduction by flowing NH_3 at various elevated temperature.

The triplet *g* value signal of N-doped TiO_2 has been further investigated by detecting the change of the signal intensity under visible light (λ = 532 nm, laser) irradiation. Fig. 4 shows the ESR spectra of N-P25(600) in the dark, after laser irradiation for 9 min, and after turning off light for 9 min. On the one hand, visible light irradiation results in increase of the intensity of the ESR spectrum as compared with that obtained in the dark, possibly because many fresh additional SETOV is generated under laser irradiation. The intensity of the triplet *g* value reaches the maximum after the light is irradiated on the sample for a few seconds, implying that the photo-excited electrons are instantaneously trapped by oxygen vacancy to achieve an equilibrium state. On the other hand, however, newly-generated SETOV will partially but not completely lose the trapped electrons (see Fig. 4c). As depicted in Schematic Diagram 1, the oxygen vacancies formed in P25-TiO_2 bulk during heat-treatment in flowing NH_3 can be hypothetically divided into three categories: SETOV with triplet *g* value signal (type-i), dual-electrons-trapped oxygen vacancy (type-ii), and oxygen vacancy without electron (type-iii). The latter two will not produce ESR signals. Under the hypothetical condition, the photo-excited electrons from valance band under irradiation will be trapped by oxygen vacancy without electron, accompanied by transfer of a single electron trapped in dual-electrons-trapped oxygen vacancy to conduction band forming fresh SETOV, resulting in increase of SETOV concentration. It is difficult for SETOV, in particular, dual-electrons-trapped oxygen vacancy, to re-capture electron, due to strong electron–electron repulsion as compared with oxygen vacancy without electron. Subsequently, when the light was turned off, some electrons would jump back to the valance band from newly-generated SETOV. However, the mobility of electrons associated with oxygen vacancy will be restricted and therefore, newly-generated SETOV will partially but not completely lose the trapped electrons. This is also observed for N-P25(500) and N-P25(700). Besides, by subtracting spectrum b from spectrum c generating Fig. 4d, we can clearly see that light irradiation can simultaneously increase the intensity of the triplet *g* value signal, which further proves that the triplet *g* value signal is attributed to single (i.e., SETOV alone) but not multiple paramagnetic species. Moreover, by assuming $\Delta_{SETOV} = h(ESR)_{light\ on} - h(ESR)_{light\ off}$, we can determine the value of Δ_{SETOV} from Fig. 4d; here Δ_{SETOV} and *h*(ESR) refer to the increased quantity of SETOV before and after laser irradiation and signal intensity at *g* = 2.004, respectively. The value of $h(ESR)_{light\ on} - h(ESR)_{light\ off}$, i.e., Δ_{SETOV} for corresponding samples are given in Fig. 5. It can be seen that Δ_{SETOV} also varies in a wave-like manner, similar to what is shown in Fig. 3. In other words, the variation of Δ_{SETOV} is linearly proportional to the visible

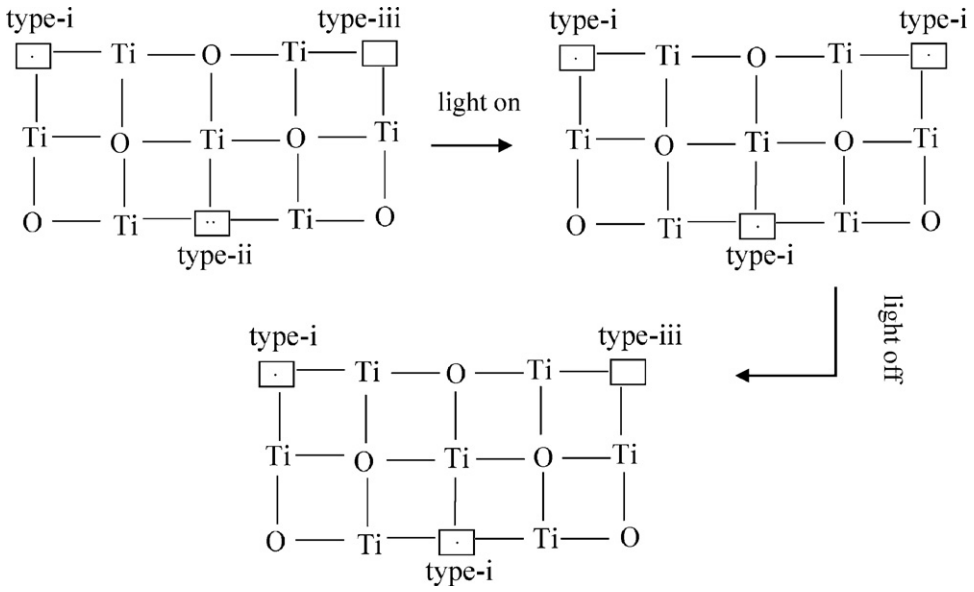

Schematic diagram 1. The process of electron transfer before/after laser irradiation (532 nm), where laser irradiation results in increase of SETOV concentration.

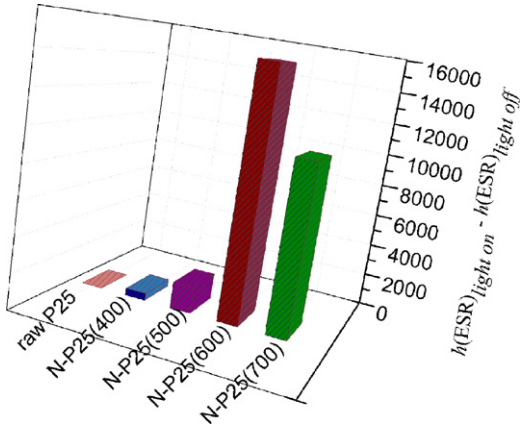

Fig. 5. Value of $h(\mathrm{ESR})_{light\ on} - h(\mathrm{ESR})_{light\ off}$ as a function of heat-treatment temperature in flowing NH_3. h(ESR) refers to the signal intensity at $g = 2.004$.

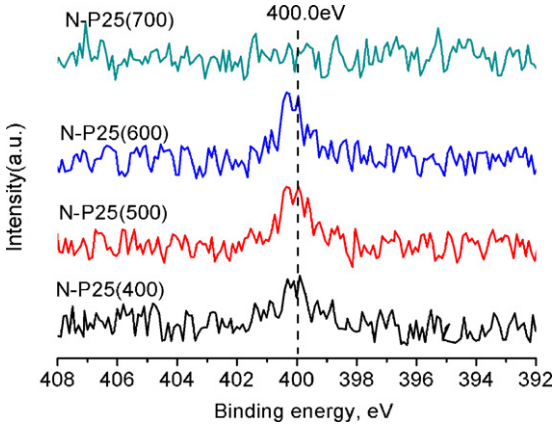

Fig. 6. N 1*s* XPS spectra of samples N-P25(400–700).

light photocatalytic activity, which further proves that the visible light photocatalytic activity of the N-doped TiO_2 is originated from SETOV.

The surface chemical composition and chemical states of N-doped TiO_2 analyzed by means of XPS are shown in Fig. 6, where the N 1*s* XPS spectra of N-P25(400–700) are provided. In terms of samples N-P25(400–600), only a single N species is detected, corresponding to N 1*s* core level binding energy (BE) of 400 eV. As to sample N-P25(700), however, no core level N 1*s* peak is detected (it has been re-confirmed by conducting repeat XPS measurements). Furthermore, the sample prepared again under the same condition also showed no N 1*s* peaks. This implies that nitrogen has not been incorporated into TiO_2 at 700 °C, possibly because of complete decomposition of NH_3 thereat. Thus it may be more reasonable to annotate sample N-P25(700) as H_2-reduced P25 but not NH_3-nitridated P25. The above observation differs from what have been reported on N 1*s* chemical states of N-doped TiO_2. Namely, Asahi and coworkers reported three N 1*s* peaks with binding energies of 402 eV, 400 eV and 396 eV and assigned them as molecularly chemisorbed γ-N_2 (BE = 402 eV and 400 eV) and atomic β-N (BE = 396 eV) according to Saha [41]. However, Sato and coworkers pointed out that the assignments of N 1*s* peaks at 402 eV and 400 eV to molecular N_2 is implausible, because at room temperature molecular N_2 is not chemisorbed on metal oxides like TiO_2 [7]. Irie and coworkers observed N 1*s* peaks of their N-doped TiO_2 at 400 eV and 396 eV and assigned them as NO and TiN, respectively [3]. Asahi et al. and Irie et al. both ascribed the 396 eV state of N-doped TiO_2 to visible light sensitization. However, many researchers observed N 1*s* peak alone at 399–400 eV and assigned it as NO; or N 1*s* peak alone at 396–397 eV assigned to N atoms in Ti–N bonds [7,42–44]. Kosowska and coworkers prepared N-doped TiO_2 catalysts by treating TiO_2 particles in gaseous NH_3 atmosphere for 4 h, in the same manner as ours but with different precursor of doped-N [13]. They evaluated the photocatalytic activity by measuring the percentage decomposition of phenol and azo-dye and obtained the highest decomposition rate with catalysts calcinated at 700 °C and 500/600 °C, respectively. Unfortunately, they did not identify the N 1*s* chemical state in their N-doped TiO_2 catalysts, nor did they explain the contribution of doped-N to the visible light sensitization.

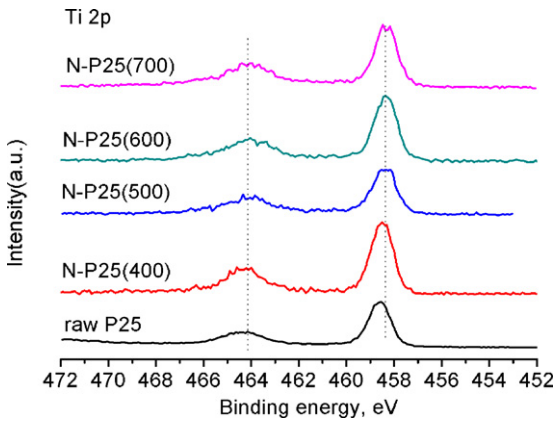

Fig. 7. Ti 2*p* XPS spectra of raw P25 and samples N-P25(400–700).

Fig. 7 shows the Ti 2*p* XPS spectra of P25 and N-P25(400–700). The spin–orbit components (Ti $2p_{3/2}$ and Ti $2p_{1/2}$) of Ti 2*p* peak are located at BE = 458.6–464.3 eV and BE = 458.4–464.1 eV for P25 and N-P25(400–700), respectively. This indicates that Ti exists as Ti^{4+} ion in the N-doped catalysts. Besides, the binding energy of samples N-P25(400–700) is slightly lower (about 0.2 eV) than that of sample P25, possibly due to difference of chemical environment of Ti^{4+} ion and more probably due to decrease of electron cloud density around Ti^{4+} ion in the N-doped samples.

Fig. 8 shows the O 1*s* XPS spectra of N-P25(400–600) and N-P25(700). It is seen that samples N-P25(400–600) show three O 1*s* peaks at 529.6 eV, 531.2 eV, and 533.3 eV. The first and second peaks can be assigned as lattice oxygen in Ti–O bond and OH groups on sample surfaces; and the third peak may arise from oxygen of NO_x [45]. However, sample N-P25(700) shows no O 1*s* peak at 533.3 eV, corresponding to its absence of N 1*s* XPS spectrum (see Fig. 6). This further verifies that no nitrogen is doped into sample N-P25(700).

A large amount of SETOV formed in a TiO_2 matrix can extend the absorption range of TiO_2 from ultraviolet region to visible light region, but it is inactive for visible light photocatalytic activity, because SETOV, *via* interaction, may act as recombination center of photogenerated e^-–h^+ [46–49]. But apparent visible light photocatalytic activity is obtained after TiO_2 is doped with N [26]. This indicates that the visible light photocatalytic activity of N-doped TiO_2 is co-determined by two factors: the formation of SETOV and presence of doped-N. The formation of SETOV in TiO_2 matrix accounts for visible light sensitization, while doped-N functions to prevent photogenerated electrons and holes from recombination, resulting in visible light photocatalytic activity. No visible light photocatalytic activity will be obtained unless the two factors function simultaneously. For example, sample N-P25(400), even though containing doped-N, still shows no visible light photocatalytic activity because of the absence of SETOV. Similarly, although sample N-P25(700) contains a large amount of SETOV, it has sharply decreased visible light photocatalytic activity, due to the disappearance of doped-N.

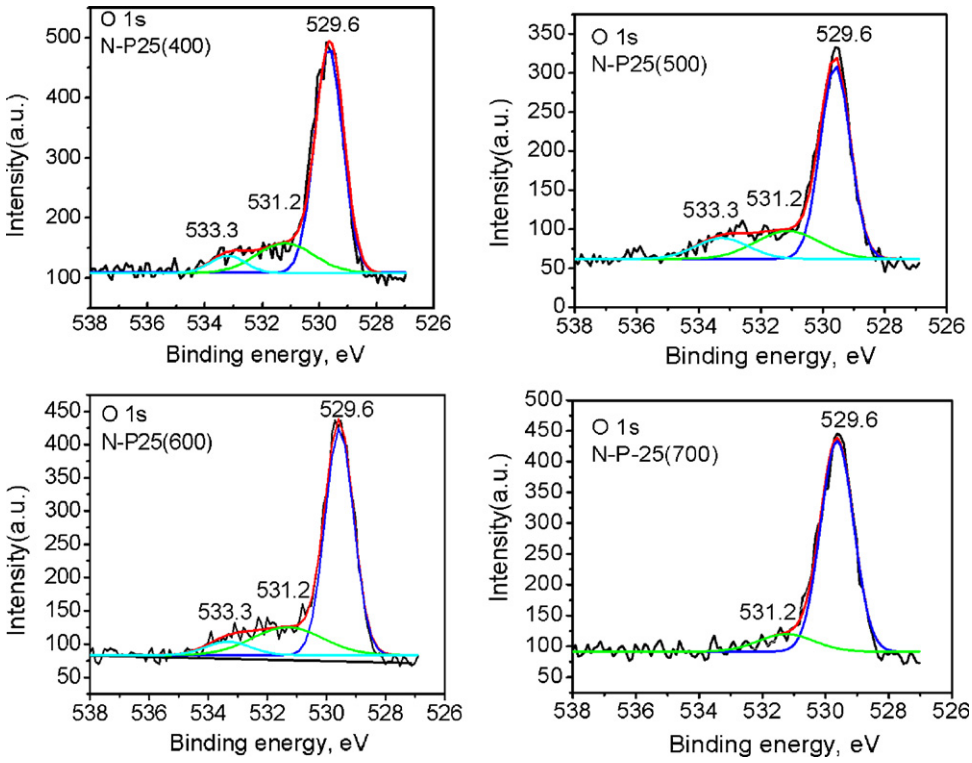

Fig. 8. O 1*s* XPS spectra of samples N-P25(400–700).

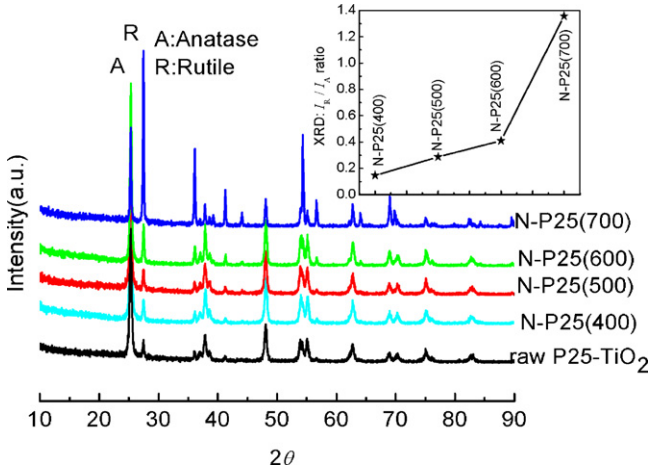

Fig. 9. XRD patterns of raw P25-TiO_2 and samples N-P25(400–700). Inset shows the variation of I_R/I_A ratio with heat-treatment temperature in flowing NH_3.

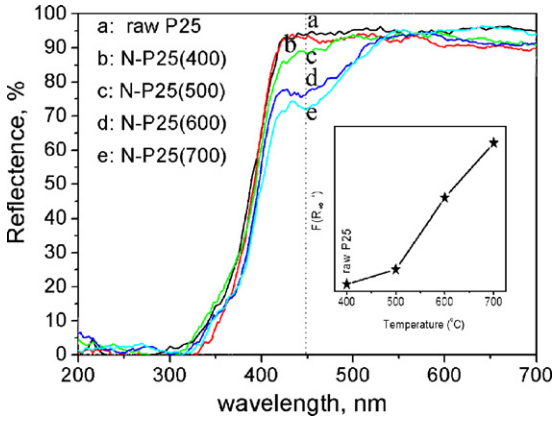

Fig. 10. Diffusion reflectance spectra of various samples: (a) raw P25-TiO_2; (b) N-P25(400); (c) N-P25(500); (d) N-P25(600); and (e) N-P25(700). Inset is the $F(R')-T$ curve; $F(R')=(1-R_\infty)^2/2R_\infty$, $F(R')$ and R_∞ refer to absorptivity and reflectance at $\lambda=450$ nm.

The XRD patterns of raw P25 and N-P25(400–700) samples are shown in Fig. 9, where the inset illustrates the variation of I_R/I_A ratio with heat-treatment temperature in NH_3 flow (I_R and I_A represent the intensity of rutile (1 1 0) and anatase (1 0 1) diffraction peaks which are the most intensive peaks for each pure phase). It can be seen that all the samples consist of mixed phases of anatase and rutile; and anatase phase is partially converted into rutile phase with the increase of temperature. Such a phase transformation is not obvious below 600 °C, but it becomes noticeable at 700 °C. This well corresponds to variation of relevant XRD data and of I_R/I_A ratio as well.

The diffusion reflectance spectra of samples N-P25(400–700) as functions of temperature are shown in Fig. 10, where the DRS spectrum of commercial P25 is also given for a comparison. It is seen that samples P25-TiO_2 and N-P25(400), due to absence of SETOV (Fig. 2), can hardly absorb visible light, which well corresponds to their poor visible light photocatalytic activity. With the increase of heat-treatment temperature in NH_3 flow, samples N-P25(500–700) possess gradually enhanced visible light absorption ability in a wavelength region of 400–520 nm. According to K–M theory [50–52], the relation between absorptivity and reflectance (R_∞) is expressed as:

$$\text{Absorptivity} = F(R') = (1-R_\infty)^2/2R_\infty$$

where R_∞ is the reflectance at a wavelength of 450 nm. The inset in Fig. 10 shows the plot of $F(R')$ versus temperature. By comparing the curve of $F(R')-T$ with that of $h_{(ESR)}-T$ shown in Fig. 3, we can further verify that the visible light absorption of N-doped TiO_2 is indeed proportional to the concentration of SETOV, the same as that reported by Zhang and coworkers [52]. Interestingly, inactive

sample N-P25(700) exhibits the strongest visible light absorption, though its concentration of SETOV is lower than that of sample N-P25(600). This may be closely related to the enhanced phase transformation from anatase to rutile at 700 °C [53,54]. In other words, the visible light absorption of sample N-P25(700) is proportional to the concentration of SETOV and the I_R/I_A ratio as well; enhanced anatase to rutile phase transformation of sample N-P25(700) results in a larger I_R/I_A ratio and hence stronger visible light absorption than sample N-P25(600).

4. Conclusions

N-doped TiO_2 (anatase/rutile) catalysts were prepared by nitridation of P25 in NH_3 flow under various temperatures, aiming at revealing the origin of their visible light response. A triplet *g* value ESR signal has been observed for as-prepared N-doped TiO_2 samples. The visible light photocatalytic activity of the N-doped TiO_2 samples is proportional to the intensity of the triplet *g* value signal, i.e., the concentration of single-electron-trapped oxygen vacancy. N-doped TiO_2 catalyst calcinated at 600 °C possesses the highest photocatalytic activity, corresponding to its maximum concentration of SETOV and strong XPS signal of core level N 1*s*. The N-doped TiO_2 catalyst calcinated at 700 °C, even though with a moderate SETOV concentration, has a sharply decreased photocatalytic activity, due to the disappearance of doped-N as evidenced by XPS analysis. This indicates that the visible light photocatalytic activity of N-doped TiO_2 is co-determined by the formation of SETOV and the presence of doped-N. The formation of SETOV in TiO_2 matrix results in visible light sensitization, while doped-N functions to prevent photoinduced electrons and holes from recombination. No visible light photocatalytic activity will be obtained for N-doped TiO_2 unless the above-mentioned two factors function simultaneously; and the higher the concentration of SETOV is, the better the visible light photocatalytic activity will be.

Acknowledgments

This work was supported by a grant from National Natural Science Foundation of China (No. 20973054). The authors would like to thank Professor Jingrong Chen for her help to measure and analyze ESR data and Professor Laigui Yu for critically reviewing the manuscript.

References

[1] S. Sato, Chem. Phys. Lett. 123 (1986) 126–128.
[2] R. Asahi, T. Morikawa, T. Ohwaki, K. Aoki, Y. Taga, Science 293 (2001) 269–271.
[3] H. Irie, Y. Watanabe, K. Hashimoto, J. Phys. Chem. B 107 (2003) 5483–5486.
[4] T. Ihara, M. Miyoshi, Y. Iriyama, O. Matsumoto, S. Sugihara, Appl. Catal. B: Environ. 42 (2003) 403–409.
[5] J. Ananpattarachai, P. Kajitvichyanukul, S. Seraphin, J. Hazard. Mater. 168 (2009) 253–261.
[6] S.Z. Hu, A.J. Wang, X. Li, H. Löwe, J. Phys. Chem. Solids 71 (2010) 156–162.
[7] S. Sato, R. Nakamura, S. Abe, Appl. Catal. A: Gen. 284 (2005) 131–137.
[8] H.Q. Sun, Y. Bai, W.Q. Jin, N.P. Xu, Sol. Energy Mater. Sol. C 92 (2008) 76–83.
[9] O. Diwald, T.L. Thompson, T. Zubkov, E.G. Goralski, S.D. Walck, J.T. Yates Jr., J. Phys. Chem. B 108 (2004) 6004–6008.
[10] Y. Wang, C.X. Feng, Z.S. Jin, J.W. Zhang, J.J. Yang, S.L. Zhang, J. Mol. Catal. A: Chem. 260 (2006) 1–3.
[11] Y. Wang, J.W. Zhang, Z.S. Jin, Z.S. Wu, S.L. Zhang, Chin. Sci. Bull. 52 (2007) 1973–1976.
[12] C.X. Feng, Y. Wang, Z.S. Jin, J.W. Zhang, S.L. Zhang, Z.S. Wu, Z.J. Zhang, New J. Chem. 32 (2008) 1038–1047.
[13] B. Kosowska, S.A. Mozia, W. Morawski, B. Grzmil, M. Janus, K. Kalucki, Sol. Energy Mater. Sol. C 88 (2005) 269–280.
[14] O. Diwald, T.L. Thompson, E.G. Goralski, S.D. Walck, J.T. Yates Jr., J. Phys. Chem. B 108 (2004) 52–57.
[15] A. Ghicov, J. M. Macak, H. Tsuchiya, J. Kunze, V. Haeablein, L. Frey, P. Schumaki, Nano. Lett. 6 (2006) 1080–1082.
[16] G. Ghicov, J.M. Macak, H. Tsuchiya, J. Kunze, V. Haeablein, S. Kleber, P. Schumaki, Chem. Phys. Lett. 419 (2006) 426–429.
[17] P.R. Vitiello, J.M. Macak, A. Ghicov, J. Tsuchiya, L.F.P. Dick, P. Schumuki, Electrochem. Commun. 8 (2006) 544–548.
[18] S. Livraghi, A. Votta, M.C. Paganini, E. Giamello, Chem. Commun. (2005) 498–500.
[19] S.M. Prokes, J.L. Gole, X.B. Chen, C. Burda, W.E. Carlos, Adv. Funct. Mater. 15 (2005) 161–167.
[20] S. Livraghi, M.C. Paganini, E. Giamello, A. Selloni, C.D. Valentin, G. Pacchioni, J. Am. Chem. Soc. 128 (2006) 15666–15671.
[21] R. Nakamura, T. Tanaka, Y. Nakato, J. Phys. Chem. B 108 (2004) 10617–10620.
[22] T. Lindgren, J.M. Mwabora, E. Avendano, J. Jonsson, C.G. Granqvist, S.E. Lindquist, J. Phys. Chem. B 107 (2003) 5709–5716.
[23] N. Serpone, J. Phys. Chem. B 110 (2006) 24287–24293.
[24] V.N. Kuznetsov, N. Serpone, J. Phys. Chem. B 110 (2006) 25203–25209.
[25] A.V. Emeline, N.V. Sheremetyeva, N.V. Khomchenko, V.K. Ryabchuk, N. Serpone, J. Phys. Chem. C 111 (2007) 11456–11462.
[26] J.W. Zhang, Y. Wang, Z.S. Jin, Z.S. Wu, Z.J. Zhang, Appl. Surf. Sci. 254 (2008) 4462–4466.
[27] S. Fukuzawa, K.M. Sancier, T. Kwan, J. Catal. 11 (1968) 364–369.
[28] R.D. Iyengar, M. Codell, J.S. Karra, J. Turkevich, J. Am. Chem. Soc. 88 (1966) 5055–5060.
[29] R.D. Iyengar, R. Kellerman, J. Colloid Interf. Sci. 35 (1971) 424–433.
[30] Y. Sakatani, J. Nunoshige, H. Ando, K. Okusako, H. Koike, T. Takata, N. Kondo, M. Hara, K. Domen, Chem. Lett. 32 (2003) 1156–1157.
[31] C.D. Valentin, G. Pacchioni, A. Selloni, S. Livraghi, E. Giamello, J. Phys. Chem. B 109 (2005) 11414–11419.
[32] S. Livraghi, A.M. Czoska, M.C. Paganini, E. Giamello, J. Solid State Chem. 182 (2009) 160–164.
[33] C. Naccache, P. Meriaudeau, M. Che, A.J. Tench, Trans. Faraday Soc. 67 (1971) 506–512.
[34] C. Naccache, Chem. Phys. Lett. 11 (1971) 323–325.
[35] A.M. Volodin, A.E. Cherkashin, V.S. Zakharenko, React. Kinet. Catal. Lett. 11 (1979) 103–106.
[36] A.M. Volodin, A.E. Cherkashin, V.S. Zakharenko, React. Kinet. Catal. Lett. 11 (1979) 107–111.
[37] E. Serwicka, M.W. Schlierkamp, R.N. Schindler, Z. Naturforch. 36a (1981) 226–232.
[38] E. Serwicka, Colloid Surf. 13 (1985) 287–293.
[39] K. Takeuchi, I. Nakamura, O. Matsumoto, S. Sugihara, M. Ando, T. Ihara, Chem. Lett. (2000) 1354–1355.
[40] T. Ihara, M. Miyoshi, J. Mater. Sci. 36 (2001) 4201–4207.
[41] N.C. Saha, H.G. Tompkins, J. Appl. Phys. 72 (1992) 3072–3079.
[42] S.K. Joung, T. Amemiya, M. Murabayashi, K. Itoh, Chem.-Eur. J. 12 (2006) 5526–5534.
[43] K. Kobayakawa, Y. Murakami, Y. Sato, J. Photochem. Photobio. A 170 (2005) 177–179.
[44] P.G. Wu, C.H. Ma, J.K. Shang, Appl. Phys. A 81 (2005) 1411–1417.
[45] J. Chastain, Handbook of X-ray Photoelectron Spectroscopy, Perkin Elmer Corporation, Minnesota, 1992.
[46] Q.Y. Li, J.W. Zhang, Z.S. Jin, D.G. Yang, X.D. Wang, J.J. Yang, Z.J. Zhang, Electrochem. Commun. 8 (2006) 741–746.
[47] Q.Y. Li, X.D. Wang, Z.S. Jin, D.G. Yang, S.L. Zhang, X.Y. Guo, J.J. Yang, Z.J. Zhang, J. Nanopart. Res. 5 (2007) 951–957.
[48] X.D. Wang, J.J. Yang, H.Y. Yin, Z.J. Zhang, Z.S. Jin, Photogr. Sci. Photochem. 20 (2002) 424–428 (in Chinese).
[49] M. Zhang, Z.S. Jin, J.W. Zhang, X.Y. Guo, J.J. Yang, W. Li, X.D. Wang, Z.J. Zhang, J. Mol. Catal. A: Chem. 217 (2004) 203–210.
[50] W.W. Wendlandt, H.G. Hecht, Reflectance Spectroscopy, Wiley Interscience, New York, 1966.
[51] J.R. Anderson, K.C. Pratt, Introduction to Characterization and Testing of Catalysts, Academic Press, Australia, 1985.
[52] S.L. Zhang, W. Li, Z.S. Jin, J.J. Yang, J.W. Zhang, Z.L. Du, Z.J. Zhang, J. Solid State Chem. 177 (2004) 1365–1371.
[53] O. Rosseler, M.V. Shankar, M.K-Le. Du, L. Schmidlin, N. Keller, V. Keller, J. Catal. 26 (2010) 179–190.
[54] S.X. Liu, X.Y. Chen, X.H. Li, Chin. J. Inorg. Chem. 24 (2008) 253–259.